Author Manuscript

Author Manuscript

Author Manuscript

Author Manuscript

HHS Public Access

Author manuscript

Nanoscale. Author manuscript; available in PMC 2020 August 07.

Published in final edited form as:

Nanoscale. 2019 August 07; 11(29): 13783–13789. doi:10.1039/c9nr02042j.

Transition structure of chromatin fibers at nanoscale probed by cryogenic electron tomography

Zhongwu Zhou[1], **Kunpeng Li**[2], **Rui Yan**[2], **Guimei Yu**[2], **Chris Gilpin**[3], **Wen Jiang**[2], **Joseph Irudayaraj**[1,4,*]

[1]Bindley Bioscience Center, Department of Agricultural and Biological Engineering, Purdue University, West Lafayette, IN 47907, USA

[2]Markey Center for Structural Biology, Department of Biological Science, Purdue University, West Lafayette, IN 47907, USA

[3]Life Science Microscopy Facility, Purdue University, West Lafayette, IN 47907, USA

[4]Department of Bioengineering, College of Engineering, 1103 Everitt Laboratory, 1406 W. Greet Street, Urbana, IL 61801, USA

Abstract

The naked DNA inside the nucleus interacts with proteins and RNAs forming higher order chromatin structure to spatially and temporally control transcription in eukaryotic cells. The 30 nm chromatin fiber is one of the most important determinants of the regulation of eukaryotic transcription. However, the transition of chromatin from the 30 nm inactive higher order structure to the actively transcribed lower order nucleosomal arrays is unclear, which limits our understanding of eukaryotic transcription. Using a method to extract near-native eukaryotic chromatin, we revealed chromatin structure at transitional state from the 30 nm chromatin to multiple nucleosomal arrays by cryogenic electron tomography (cryo-ET). Reproducible electron microscopy images revealed that the transitional structure is a branching structure that the 30 nm chromatin hierarchically branches into lower order nucleosomal arrays, indicating chromatin compaction at different levels to control its accessibility during interphase. We further observed that some of the chromatin fibers on the branching structure have a helix ribbon structure, while the others randomly twist together. Our finding of chromatin helix ribbon structure on extracted native chromatin revealed by cryo-ET indicates a complex higher order chromatin organization beyond the beads-on-a-string structure. The hierarchical branching and helix ribbon structure may provide mechanistic insights into how chromatin organization plays a central role in transcriptional regulation and other DNA-related biological processes.

Introduction

The about two meters of naked genomic DNA packed in the human nucleus decorated with histone and non-histone proteins and RNAs, folds into hierarchical chromatin structures

*Corresponding author: Joseph Irudayaraj (jirudaya@illinois.edu).

Conflicts of interest

There are no conflicts to declare.

Author Manuscript Author Manuscript Author Manuscript Author Manuscript

during interphase which includes the 10 nm “beads-on-a-string” nucleosomal array[1, 2], 30 nm chromatin fibers, and with contention, thicker fibers with diameters beyond 30 nm[3]. The compaction levels of chromatin play a fundamental role in the regulation of gene transcription and all other biological processes, such as DNA replication, repair and recombination[4]. The 30 nm chromatin fiber is the first level of transcriptionally dormant chromatin, whose critical function might be to regulate the accessibility of transcription factors via dynamic transitions between the more compact 30 nm chromatin fiber in heterochromatin and more accessible lower order 10 nm chromatin structure[5]. However, the transition structure between the 30 nm higher order inactive heterochromatin and the actively transcribed lower order euchromatin is not clearly understood.

Resolving this transition structure requires both preparation of chromatin samples that maintains the hierarchically 30 nm structures and experimental techniques that can directly visualize the chromatin with nano-scale resolution. Cryogenic electron microscope (Cryo-EM) single particle method with ~1 nm resolution has been utilized to study the structure of 30 nm chromatin fiber using uniform, *in vitro* reconstituted short pieces of chromatin, which revealed that the helical ribbon structure of 30 nm chromatin fiber is a histone H1-dependent left-hand twist of the repeating tetra-nucleosomal structural units[6]. However, due to the requirement of repeated uniform individual complex in single particle method, this technique cannot be applied to study the transitional state of 30 nm chromatin fiber and 10 nm chromatin fiber. ChromEMT, an electron-microscopy-based method, provided nano-scale images of sectioned eukaryotic interphase chromatin structures, revealing that the chromatin is flexible and has a disordered 5-24 nm granular chain in interphase nuclei[7]. However, due to the complexity of chromatin looping in the 3D nuclei, the images of sectioned chromatin also cannot resolve the mentioned transition state structure. Moreover, the heavy crosslinking and staining process are well known to damage the secondary structure of large DNA complexes[8]. This could explain why the classic helical ribbon structure of the 30 nm chromatin fiber was not detectable by ChromEMT. Optical super-resolution microscopy has been applied to determine the structure of chromatin inside the nucleus down to ~20-30 nm resolution[9-12], however, resolving the twisted lower order 10 nm nucleosomal arrays is challenging.

Cryogenic electron tomography (cryo-ET) is a powerful tool to bridge the resolution gap between the molecular structures of individual proteins as revealed by cryo-EM single particle anlaysis and larger cellular architectures as observed by optical microscopy[13]. However, due to the condensed nature of chromatin as well as weak contrast between chromatin and its surrounding proteins and ions, only sparse information could be obtained from cryo-ET studies of the sectioned nuclei[14, 15]. We have addressed these problems by extracting mammalian chromatin and further using cryo-ET to observe its near-native structure in vitreous ice. We observed that the interphase chromatin consists of DNA compacted at different hierarchically levels, at the simplest branching order the 30 nm chromatin fiber is observed to bifurcate into multiple 10 nm beads-on-a-string nucleosomal arrays We have also observed that some chromatin fibers on the branching structure form a helical structure while others randomly twist together. The observed branching and helix structures may provide additional insights into the relationship between chromatin structure and DNA regulation during interphase.

Author Manuscript Author Manuscript Author Manuscript Author Manuscript

Results and Discussion

Preparation of Chromatin sample for structural analysis

Higher order chromatin structure inside eukaryotic nucleus is hierarchically packaged into multiple levels[4, 5, 16]. While multiple microscopic methods with different resolution limits can investigate higher order chromatin structure, less detailed information on how higher order structure transitions into lower order structure is available. This is due in part to the limitations of current techniques used in the isolation and preparation of intact chromatin. To resolve the transitional state structure, we developed a method to extract intact interphase chromatin by a solid phase reversible immobilization (SPRI) method using salicylic acid coated magnetic nanoparticles (SAMNPs) as carriers[17]. The chromatin extracted by SPRI method is different from the soluble fragmented chromatin extracted by conventional methods[18-20] and from the *in vitro* reconstituted short nucleosomal arrays[6, 21, 22] in terms of chromatin fiber length and integrity. The extracted chromatin fibers demonstrated a strong DNA adsorption peak at 260 nm, as shown in Fig. 1A. We observed morphological distinction between isolated DNA and chromatin which falls in line with our previous study[17]. When directly mounted on the continuous carbon surface of EM grids, the chromatin fibers easily intertwined together to form the tangled globule-like structures as shown in Figure 1B. The globular chromatin structure is commonly observed in other microscopic studies[22-24]. It is reported that this tangled globular structure is highly related to the contracting domains identified by Hi-C[25-2728], and is the form mammalian chromosomes organize into during interphase[28]. Interestingly, *in vitro* reconstituted nucleosomal arrays are also packed into globular structures in size range from ~50 nm to a maximum diameter of ~1000 nm[22]. The observed globular chromatin in this study has high similarity to the reported globular structure inside the nucleus and *in vitro* reconstituted chromatins, suggesting that our extracted chromatin are good *in vitro* model systems for studying the interphase chromosome structure and organization. However, using a buffer flow the chromatin aligns into a characteristically distinct morphology demonstrating a bifurcated hierarchical structure as shown in Figure 1C. The length of extracted chromatin (Fig. 1C) was observed to reach 100 μm on a 200-mesh continuous carbon film coated EM grid. This type of chromatin morphology is consistent with our previous characterization by atomic force microscopy (AFM)[17] , which uses flowing buffers to clean the mica surface, allowing the chromatin fibers to align on the mica before AFM imaging. The aligned chromatin clearly shows a hierarchical branching structure. We can identify at least four levels of branching structure (Fig. S1), among them; the 30 nm chromatin fiber is the penultimate structure, before further unwinding into multiple 10 nm beads-on-a-sting nucleosomal arrays. We define the 30 nm chromatin branching structure and its immediate branching nucleosomal arrays as the transitional 30 nm chromatin branching structure. Obviously, the 10 nm chromatin fibers are much more assessable compared to the 30 nm chromatin fiber which contains highly dense DNA. Thus, the transitional 30 nm chromatin branching structure might represent the intermediate transition structure between compact heterochromatic chromatin and open translatable chromatin. Moreover, the typical beads-on-a-string structure of the extended chromatin was also clearly observed at a higher magnification (Fig.1D), which is also consistent with our previous AFM studies[17].

Author Manuscript Author Manuscript Author Manuscript Author Manuscript

Chromatin fibers are generally insoluble under physiological salt conditions; however, its solubility increases with increased ionic strength. The ionic surfactant, sodium dodecyl sulfate (SDS), which can not only promote protein solubility but also provide sufficient ionic strength, was chosen to dissolve the chromatin[29, 30]. Nonionic surfactant, such as Triton X-100, can form micelles, which promote protein solubility, but cannot dissolve chromatin even at concentration of 10% (m/v)[29]. According to Zhang et al[30], 250 mM SDS lysis buffer is shown to dissolve the released chromatin successfully. Interestingly, we extracted chromatin fibers successfully using 25 mM SDS by the SPRI method, and did not notice any significant structural difference regarding the chromatin morphology as seen in Figure 1B. A slight loss of weakly associated proteins was noticed during the extraction procedure using 250 mM SDS [30], however, when with 25 mM SDS, we successfully prepared clean negative stain TEM images that show regularly spaced “nucleosome-like” particles along the 10 nm chromatin fiber (Fig. 1D) like a replication fork. Slow pipetting was performed to minimize the mechanical shear force on the chromatin fibers. Pre- and post-crosslinking by paraformaldehyde or glutaraldehyde was avoided so as to not disturb the native epigenetic profiles that cause structural changes in chromatin[31-33]. Since its epigenetic profile is not altered during extraction, the epigenetic marks including DNA modifications and histone modifications of the extracted chromatin can be directly measured at global level[34]. Moreover, without aldehyde fixation, we exclude the suspicion that the 30 nm fibers are an artifact of the fixation process[35, 36]. Salt concentration affects higher order chromatin structure[37], for example, the DNA conformation might vary among extended chromatin (10 mM NaCl), compacted chromatin (50 mM NaCl), solenoidal chromatin (100 mM NaCl), and aggregated chromatin (150 mM NaCl) [38]. We were interested in studying the higher order chromatin structures in the latter condition, so that the chromatin is maintained at the physiological salt condition using a 1x PBS containing 1 mM $MgCl_2$, which was used to stabilize the nucleosome[22, 39]. In the range of 0-2 mM $MgCl_2$, chromatin fiber remains its initial state without forming artificial oligomerization. The methods implemented for isolating and preparing chromatin were all at physiological concentrations, hence the observed structures are in native form and could be used for additional characterization[20].

Plunge-freezing chromatin sample for cryo-ET

Due to the high viscosity and large size of the concentrated chromatin fibers, cryogenic freezing of the chromatin on holey carbon films such as C-flat and Quantifoil was challenging. Either no chromatin was observed or chromatin fibers embedded in the thick vitreous ice, obstructed the electrons and impeded the tomographic image acquisition. Moreover, the chromatin fibers are inherently tangled together in the form of globular structures as shown in Figure 1B. These challenges were resolved by manual blotting of liquid chromatin samples from the edge of the grids. Again, the manual blotting from the edge of the holey grid introduces a mild force within the liquid to align the chromatin fibers which reduces the tangling of the chromatin fibers and allows the finer structures to be observed on lacey carbon coated EM grids.

Transitional 30 nm chromatin branching structure

Cellular chromatin was extracted using the SPRI method with SAMNPs and the conditions were optimized for freezing chromatin samples in vitreous ice. Cryogenic electron

Author Manuscript Author Manuscript Author Manuscript Author Manuscript

tomography data collected represents chromatin fiber under different levels of compaction. From these tomographic date sets, two data sets were selected and further 3D reconstructed. They consistently present the transitional 30 nm chromatin branching structure, which has been observed in negative staining EM. Instead of embedding in heavy metal and exposing to dehydrating conditions in negative staining EM, the chromatin were preserved in vitreous ice at near native state, which facilitates observation of finer structures. As mentioned before, this complexity is defined as the transitional 30 nm chromatin branching structure. In vitreous ice DNA molecules have higher contrast than the background [20, 40, 41], making the chromatin fiber easy to visualize, as shown in Fig. 2A (Branching 1) and Fig. 3A (Branching 2). The electron microscope stage was tilted from −56 degree to +56 degree, and images were collected every two degrees at the position of interest. The collected cryo-ET data set was further reconstructed into 3D structure by IMOD. The resolution of the 3D reconstruction for 4-time binned Branching 2 was determined ~10 nm. The cryo-ET 3D reconstruction confirmed that the observed branching structure consists of several nucleosomal arrays bifurcating from a single 30 nm trunk (Figure 2 and Figure 3; ESI Movie 1 and ESI Movie 2), ruling out the possibility that the observation is an artifact caused by the overlap of two distinct chromatin fibers. A tomographic slice of the 3D structure (Fig. 2B or Fig. 3B) clearly indicates that the transition structure between the 30 nm chromatin fiber and the nucleosomal arrays is a branching structure. Here, we termed the thick region on the branching structure as the “root”, and the thin regions as “branches”. The thickness of the root is approximately 31 nm in Branching 1 and 39 nm in Branching 2. According to Robinson et al[42], the 30 nm chromatin fiber has a diameter ranging from 30 nm to 40 nm, thus the observed two transitional chromatin structures were within the range of 30 nm chromatin fiber. The thickness of the nucleosmal arrays of the branches varies from 10 nm to 20 nm due to its twist to another. The branching structure indicates how the basic 10 nm nucleosomal arrays organize into 30 nm chromatin fibers. In branching 1 (Figure 2C), four DNA molecules organize into two branches and then further compact by twisting together forming the 30 nm chromatin fiber with a thickness of 31 nm. The 30 nm chromatin fiber containing four DNA molecules, is different from the reported *in vitro* reconstituted 30 nm fiber, which contains only two DNA molecules[6]. Though its detailed structure needs to be further elucidated, the observations provide a new paradigm for higher order chromatin structure.

Chromatin requires multiple levels of condensation and folding to compact into the nucleus[43], which when necessary will open and unwind to orchestrate replication and transcription. The transitional branching structure from 30 nm chromatin fiber to lower order nucleosomal arrays is a good example of a structure which can meet these demands. Genes located at the root (which might be heterochromatin) are possibly silenced, while genes located in the loosely compacted branches (which might be euchromatin) would have a higher chance of being expressed. Moreover, the 30 nm fibers might have various conformational states that are involved in the transition from inactive heterochromatin to active euchromatin. However, detailed molecular mechanism regulating the conformational change of the 30 nm chromatin fiber still needs to be understood.

Author Manuscript Author Manuscript Author Manuscript Author Manuscript

Chromatin helix ribbon structure at local level

Through the 3D reconstruction of Branching 2, we observed that there is a short-range helical structure on one of the chromatin branches (Fig. 3D; ESI Movie 2;). The precise path of the DNA in the helical structure is clearly observed in the tomographic slices of the reconstructed 3D chromatin branching structure (Fig. 3D). The histone and/or other non-histone proteins were also visible on the density map but omitted due to the resolution cut off. This kind of short-range helical structure is also observed at the end of one of the branches in Fig. 2C (ESI Movie 1). Compared to the Li-Zhu style "double double helix model"[6], the length of the helical structure in Figure 2 and 3 ranges from 400 nm to 600 nm, which is significantly longer than the *in vitro* reconstituted helical structure. However, the average length of each helix turn is 57.5 nm, which is in good agreement with the Li-Zhu model, Table 1. Interestingly, the thickness of the two helical ribbon structures is different from each other, and significantly smaller compared to the Li-Zhu style helical model. This variation might be because the linker DNA length varies in the helical structure of the extracted chromatin, which is different from the *in vitro* reconstituted 30 nm chromatin fiber using defined DNA repeat and uniform histone composition. The various linker DNA length in native chromatin might result from epigenetic modifications on DNA or histone tails and variants of the core and linker histones[44]. According to space-filling models, the minimum linker length allowed for the 30 nm ribbon formation is 10 bp (3.4 nm), resulting in a nucleosome repeat of at least 176 bp. The observed helical ribbon structure has a linker DNA length larger than this by about three times. The linker DNA in branching 1 (Fig. 3A) seems stretched, while the linker DNA in branching 2 (Fig. 3B) appears relaxed. This phenomenon might be due to the difference in the linker DNAs[45]. H1 protein molecules, which can interact directly with each other, play an important role in the formation of the helical ribbon structure by imparting an additional twist between each helical structural unit. However, due to the missing wedge of electron tomography, we cannot exactly identify them from the reconstructed density map. Heterochromatin Protein 1 (HP1), which plays an important role in long-term gene silencing by forming constitutive/heterochromatin, by either directly binding to methylated H3K9 through its chromodomain or recruiting other HP1 proteins through its chromo shadow domain[46, 47]. Recently, the structural model for HP1 binding to dinucleosomes propose that the dimeric HP1α, like a bridge, bind two adjacent nucleosomes with both containing H3K9me3s[48]. However, we could not identify any extra electron density between any two adjacent nucleosomes in the helical ribbon structure. Thus, HP1 as a constitutive heterchromatin mark might not exist on the helical ribbon structure.

For fibres located in the same branching structure with similar size, some formed the helical ribbon structure while others formed the random twist (Fig. 3). This has been frequently observed in our studies. Therefore, we speculate that both the highly compacted helical ribbon structure and the loosely compacted random twist co-exist in the nucleus during interphase. Whether the helical ribbon structure is the primary form of architecture on the branching structure is still an open question[20]. The coexistence of compact and loose chromatin fiber provides structural interpretation for gene activity control. Transcriptionally silent chicken erythrocyte chromatin, which is a 30 nm helical ribbon structure, differs from constitutive heterochromatin in terms of epigenetic modification profile and absence of HP1

Author Manuscript Author Manuscript Author Manuscript Author Manuscript

(heterochromatin mark)[49]. This is consistent with our results indicating that the HP1 is not on our observed helical ribbon structure. Thus, it is reasonable to speculate that this type of helical fiber organization may be more representative of facultative heterochromatin, which can transit between the open and close states to play a role in gene expression and suppression, respectively. The loosely twisted chromatin fiber might transit from the compact helical ribbon structure by chromatin remodelling, in which the original DNA/histone marks were altered[50]. There are more than 1,000 chromatin-associated proteins, and most of them are involved in chromatin remodelling, including DNA modification enzymes (DNMT1[51], DNMT3A[52], and TET[53] etc) and histone modification enzymes (KDM5[54], PRDM9[55], SET domain proteins[56] and GCN5[57] etc). Depleting the corresponding chromatin remodelers to alter the epigenetic marks on the helical ribbon structure might cause a significant change in the helical structure. However, currently the understanding of the epigenetic marks on the helical structure is limited, which needs further investigation. We also need to point out that before these chromatin remodelers (epigenetic writer or eraser) perform its function, the reader should recognize and first contact the original marks on the helical structure.

Conclusions

We address the transition structure from inactive chromatin fiber branching into accessible nucleosomal arrays in its near-native state in interphase using cryo-ET. With high-resolution electron microscopy imaging we reveal that chromatin compacts DNA at different levels during interphase. The transition between the 30 nm chromatin fiber and lower order bead-on-a-string nucleosomal array is a hierarchical branching structure. 3D reconstruction of the branching structure at nano-scale resolution reveals that some of the fibers have a helical ribbon structure, which is consistent with the *in vitro* reconstituted chromatin, while others randomly twist together. The 30 nm chromatin fiber with a helical ribbon structure is speculated to be facultative chromatin, and provides structural interpretation for local gene activity control. Our study of the transitional branching chromatin structure sheds light on the architecture of structural conformation of chromatin during interphase.

Experimental

Native chromatin extraction

Human MCF7 cells were cultured using standard protocols. The cells were synchronized at interphase by serum starvation. Chromatin was extracted by optimized solid phase reversible immobilization (SPRI) method using salicylic acid coated magnetic nanoparticles (SAMNPs) as carriers. Briefly, the cells were enriched by magnetic separation, and lysed in buffer containing 25 mM SDS, 1 mM EDTA, 1 mM PMSF, 0.5 mM EGTA and 2% protease inhibitor Cocktail in PBS 1x containing 1 mM $MgCl_2$. The mixture was pipetted up and down slowly 20 times with a 200-μl pipette tip and further incubated for 10 min. Isopropanol was added to the suspension to form nucleic acids-SAMNPs complexes and incubated for another 5 min on ice. The chromatin-SAMNPs complexes were isolated by an external magnetic field, and quickly washed one time with 1x PBS. Chromatin was eluted in a 50 μl 1x PBS buffer containing 1 mM $MgCl_2$ for 4h. The released chromatin in supernatant was

Author Manuscript Author Manuscript Author Manuscript Author Manuscript

collected after a second magnetic separation. The concentration of chromatin was determined from DNA absorbance at 260 nm in 1x PBS by NanoDrop Spectroscopy.

Negative staining EM sample preparation and data collection

The extracted chromatin samples with a concentration of 50 ng/μl were used for negative stained electron tomography data collection. 10 μl of chromatin sample was mixed with 10 μl of 16 nm gold nanoparticle solution. An aliquot of 4 μl of the mixture was adsorbed onto the glow-discharged 200 mesh carbon continuous grids (Ted Pella, INC, CA, USA) for 1 min, manually blotted by putting a piece of #1 filter paper on the edge of the grid, and stained with 4 μl of uranyl acetate (UA, 2%) for 10s. After removing the UA, the grids were briefly washed with 4 μl water and further air dried. The grids were transferred into an FEI T20 electron microscope (FEI, Eindhoven) equipped with a LaB6 filament and operated at 200 kV. Negative stained micrographs of chromatin samples were obtained using a Gatan camera at different magnification according to the size of different chromatin fibers.

Cryo-ET grid preparation

The extracted chromatin samples with a concentration of 220 ng/μl were used for freezing. 10 μl of chromatin sample was mixed with 12 μl of 10 nm gold nanoparticle solutions. An aliquot of 3 μl of the mixture was adsorbed onto the glow-discharged 400 mesh Lacey carbon holey grids (Ted Pella, INC, CA, USA) for 1 min, and then manually blotted by putting a piece of #1 filter paper at the edge of the grid at 50% humidity, followed by plunging into liquid ethane cooled by liquid nitrogen inside an FEI Vitrobot Mark III (FEI, Eindhoven).

Cyro-ET data collection and 3D reconstruction

The grids were transferred into an FEI Titan Krios electron microscope (FEI, Eindhoven) equipped with a field emission gun and operated at 300 kV. Cryo-EM micrographs of chromatin samples were obtained using a K2 direct electron director and at 11,000x nominal magnification corresponding to a pixel size of 1.3 Å/pixel. The tomographic images of the chromatin branching structure were automatically recorded using Leginon[58]. The nominal defocus was set to −4 μm for all sessions. An angular range was set to −56 to +56 degree with increments of 2 degree. Before image acquisition, the microscope was carefully aligned at a reference position. The total dosage for each tomography series was set to ~ 80 e-/Å2, and the dose for each tilt was approximately 0.98 e-/$Å^2$. Before image processing, the sub-frames at each tilt angle were motion corrected and then averaged. The averaged tilted images were stacked into a series by *newstack* and *addtostack* functions (IMOD)[59]. All tomographic reconstructions were obtained with the program IMOD (http://bio3d.colorado.edu/)[60].

Supplementary Material

Refer to Web version on PubMed Central for supplementary material.

Author Manuscript Author Manuscript Author Manuscript Author Manuscript

Acknowledgements

We thank Drs. Arnold Stein, Guohong Li and Chris Woodcock for their helpful discussions during the experimental design and manuscript preparation. We also appreciate Dr. Clayton B. Woodcock for critical reading. This project was partly funded by the W.M. Keck Foundation grant and the Indiana Clinical and Translational Sciences Institute funded, in part by Grant Number (TR000006) from the NIH. Part support from the USDA-ARS project number 935-42000-049-00D in conjunction with the Center for Food Safety Engineering at Purdue University is appreciated.

References

1. Olins AL and Olins DE, Science, 1974, 183, 330–332. [PubMed: 4128918]
2. Woodcock CL, Safer JP and Stanchfield JE, Exp Cell Res, 1976, 97, 101–110. [PubMed: 812708]
3. Belmont AS and Bruce K, The Journal of Cell Biology, 1994, 127, 287–302. [PubMed: 7929576]
4. Li G and Reinberg D, Current opinion in genetics & development, 2011, 21, 175–186. [PubMed: 21342762]
5. Li G and Zhu P, FEBS letters, 2015, 589, 2893–2904. [PubMed: 25913782]
6. Song F, Chen P, Sun D, Wang M, Dong L, Liang D, Xu R-M, Zhu P and Li G, Science, 2014, 344, 376–380. [PubMed: 24763583]
7. Ou HD, Phan S, Deerinck TJ, Thor A, Ellisman MH and O'shea CC, Science, 2017, 357, eaag0025. [PubMed: 28751582]
8. Chen C, Lim HH, Shi J, Tamura S, Maeshima K, Surana U and Gan L, Molecular biology of the cell, 2016, 27, 3357–3368. [PubMed: 27605704]
9. Xu J, Ma H, Jin J, Uttam S, Fu R, Huang Y and Liu Y, Cell reports, 2018, 24, 873–882. [PubMed: 30044984]
10. Wang Y, Maharana S, Wang MD and Shivashankar GV, Scientific Reports, 2014, 4, 4477. [PubMed: 24667378]
11. Ricci MA, Manzo C, García-Parajo MF, Lakadamyali M and Cosma MP, Cell, 2015, 160, 1145–1158. [PubMed: 25768910]
12. Fang K, Chen X, Li X, Shen Y, Sun J, Czajkowsky DM and Shao Z, ACS nano, 2018, 12, 4909–4918. [PubMed: 29715004]
13. Milne JLS, Borgnia MJ, Bartesaghi A, Tran EEH, Earl LA, Schauder DM, Lengyel J, Pierson J, Patwardhan A and Subramaniam S, The FEBS journal, 2013, 280, 28–45. [PubMed: 23181775]
14. Eltsov M, MacLellan KM, Maeshima K, Frangakis AS and Dubochet J, Proceedings of the National Academy of Sciences, 2008, 105, 19732–19737.
15. Li X, Feng H, Zhang J, Sun L and Zhu P, Biophysics Reports, 2015, 1, 51–60. [PubMed: 26942219]
16. Bascom G and Schlick T, Biophysical journal, 2017, 112, 434–445. [PubMed: 28153411]
17. Zhou Z and Irudayaraj J, Analyst, 2015, 140, 938–944. [PubMed: 25475154]
18. Oudet P, Gross-Bellard M and Chambon P, Cell, 1975, 4, 281–300. [PubMed: 1122558]
19. Suau P, Bradbury EM and Baldwin JP, European Journal of Biochemistry, 1979, 97, 593–602. [PubMed: 467433]
20. Woodcock CL, Frado LL and Rattner JB, J Cell Biol, 1984, 99, 42–52. [PubMed: 6736132]
21. Rogge RA, Kalashnikova AA, Muthurajan UM, Porter-Goff ME, Luger K and Hansen JC, Journal of Visualized Experiments : JoVE, 2013, DOI: 10.3791/50354, 50354.
22. Maeshima K, Rogge R, Tamura S, Joti Y, Hikima T, Szerlong H, Krause C, Herman J, Seidel E, DeLuca J, Ishikawa T and Hansen JC, The EMBO journal, 2016, 35, 1115–1132. [PubMed: 27072995]
23. Scheer U, Sommerville J and Müller U, Experimental Cell Research, 1980, 129, 115–126. [PubMed: 7428809]
24. The Cell Nucleus, Scheer U, Zentgraff H, Busch H and Rothblum L, 1982, vol. 11, 143–176.
25. Mirny LA, Chromosome research, 2011, 19, 37–51. [PubMed: 21274616]

Author Manuscript Author Manuscript Author Manuscript Author Manuscript

26. Fudenberg G and Mirny LA, Current Opinion in Genetics & Development, 2012, 22, 115–124. [PubMed: 22360992]
27. Sanyal A, Baù D, Martí-Renom MA and Dekker J, Current opinion in cell biology, 2011, 23, 325–331. [PubMed: 21489772]
28. Hansen JC, Connolly M, McDonald CJ, Pan A, Pryamkova A, Ray K, Seidel E, Tamura S, Rogge R and Maeshima K, Biochemical Society Transactions, 2018, 46, 67–76. [PubMed: 29263138]
29. Zhang Y, Hu Z, Qin H, Liu F, Cheng K, Wu R. a. and Zou H, Analytical Chemistry, 2013, DOI: 10.1021/ac401269g.
30. Zhang Y, Hu Z, Qin H, Wei X, Cheng K, Liu F, Wu R. a. and Zou H, Analytical Chemistry, 2012, 84, 10454–10462. [PubMed: 23121485]
31. Mohieldin AM, AbouAlaiwi WA, Gao M and Nauli SM, Scientific Reports, 2015, 5, 15982. [PubMed: 26521680]
32. Cuddapah S, Barski A, Cui K, Schones DE, Wang Z, Wei G and Zhao K, Cold Spring Harbor Protocols, 2009, 2009, pdb.prot5237.
33. Cheng Y, Grigorieff N, Penczek PA and Walz T, Cell, 2015, 161, 438–449. [PubMed: 25910204]
34. Zhou Z, Cho I-H, Shan Z and Irudayaraj J, Analytical Chemistry Research, 2015, 4, 39–44.
35. Chalkley R and Hunter C, Proceedings of the National Academy of Sciences, 1975, 72, 1304–1308.
36. Kuznetsova MA and Sheval EV, Cell biology international, 2016, 40, 1140–1151. [PubMed: 27569720]
37. Allahverdi A, Chen Q, Korolev N and Nordenskiöld L, Scientific reports, 2015, 5, 8512. [PubMed: 25688036]
38. Almagor M and Cole R, Journal of Biological Chemistry, 1989, 264, 6515–6519. [PubMed: 2703503]
39. Ni X and Cole RD, Biochemistry, 1994, 33, 9276–9284. [PubMed: 8049228]
40. Dubochet J, Bednar J, Furrer P and Stasiak A, in Nucleic Acids and Molecular Biology, Springer, 1994, pp. 41–55.
41. Furrer P, Bednar J, Dubochet J, Hamiche A and Prunell A, Journal of Structural Biology, 1995, 114, 177–183. [PubMed: 7662486]
42. Robinson PJ, Fairall L, Huynh VA and Rhodes D, Proceedings of the National Academy of Sciences, 2006, 103, 6506–6511.
43. Chen P, Zhu P and Li G, Protein & Cell, 2014, 5, 489–491. [PubMed: 24969419]
44. Scheffer MP, Eltsov M and Frangakis AS, Proceedings of the National Academy of Sciences, 2011, 108, 16992–16997.
45. Worcel A, Strogatz S and Riley D, Proceedings of the National Academy of Sciences, 1981, 78, 1461–1465.
46. Jacobs SA, Taverna SD, Zhang Y, Briggs SD, Li J, Eissenberg JC, Allis CD and Khorasanizadeh S, The EMBO Journal, 2001, 20, 5232–5241. [PubMed: 11566886]
47. Cowieson NP, Partridge JF, Allshire RC and McLaughlin PJ, Current Biology, 2000, 10, 517–525. [PubMed: 10801440]
48. Watanabe S, Mishima Y, Shimizu M, Suetake I and Takada S, Biophysical Journal, 2018, 114, 2336–2351. [PubMed: 29685391]
49. Gilbert N, Boyle S, Sutherland H, de Las Heras J, Allan J, Jenuwein T and Bickmore WA, The EMBO journal, 2003, 22, 5540–5550. [PubMed: 14532126]
50. Tse C, Sera T, Wolffe AP and Hansen JC, Molecular and Cellular Biology, 1998, 18, 4629–4638. [PubMed: 9671473]
51. Cheng X and Blumenthal RM, Structure (London, England : 1993), 2008, 16, 341–350.
52. Jia D, Jurkowska RZ, Zhang X, Jeltsch A and Cheng X, Nature, 2007, 449, 248. [PubMed: 17713477]
53. He Y-F, Li B-Z, Li Z, Liu P, Wang Y, Tang Q, Ding J, Jia Y, Chen Z and Li L, Science, 2011, 333, 1303–1307. [PubMed: 21817016]

Author Manuscript Author Manuscript Author Manuscript Author Manuscript

54. Horton JR, Engstrom A, Zoeller EL, Liu X, Shanks JR, Zhang X, Johns MA, Vertino PM, Fu H and Cheng X, Journal of Biological Chemistry, 2016, 291, 2631–2646. [PubMed: 26645689]

55. Koh-Stenta X, Joy J, Poulsen A, Li R, Tan Y, Shim Y, Min J-H, Wu L, Ngo A and Peng J, Biochemical Journal, 2014, 461, 323–334. [PubMed: 24785241]

56. Dillon SC, Zhang X, Trievel RC and Cheng X, Genome biology, 2005, 6, 227. [PubMed: 16086857]

57. Lee KK and Workman JL, Nature reviews Molecular cell biology, 2007, 8, 284. [PubMed: 17380162]

58. Suloway C, Pulokas J, Fellmann D, Cheng A, Guerra F, Quispe J, Stagg S, Potter CS and Carragher B, Journal of Structural Biology, 2005, 151, 41–60. [PubMed: 15890530]

59. Kremer JR, Mastronarde DN and McIntosh JR, Journal of Structural Biology, 1996, 116, 71–76. [PubMed: 8742726]

60. Mastronarde DN, Journal of Structural Biology, 1997, 120, 343–352. [PubMed: 9441937]

Author Manuscript Author Manuscript Author Manuscript Author Manuscript

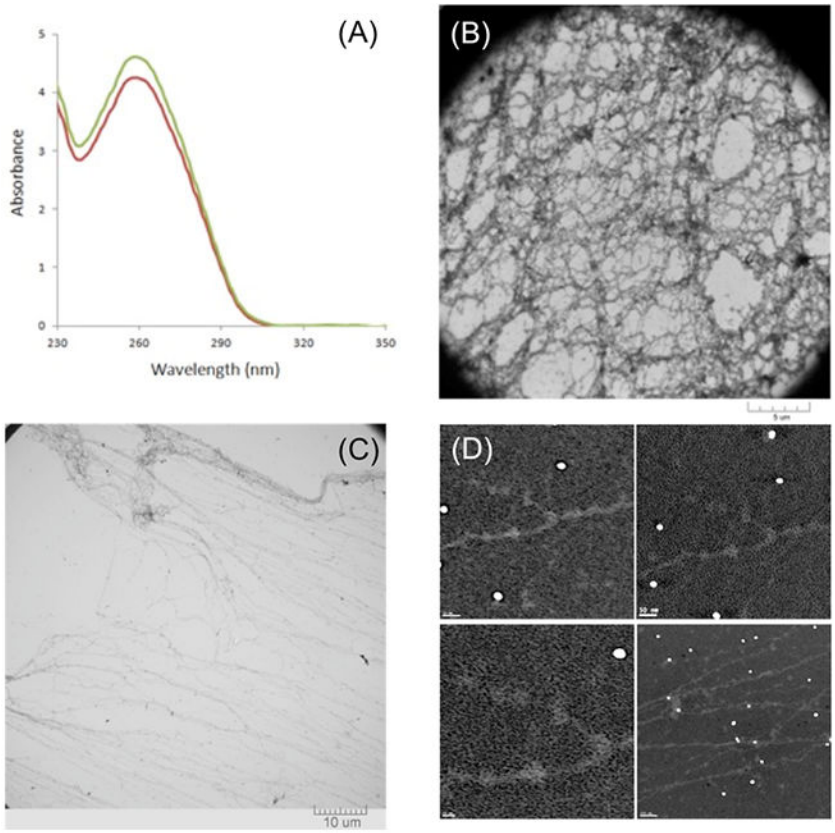

Figure 1.

(A) The absorption spectra of extracted chromatin. Chromatin with a concentration (220 ng/μl) was measured twice using Nanodrop. (B) Tangled chromatin exhibits globule-like structure. When directly mounting the extracted chromatin on the continuous carbon coated EM girds without buffer alignment, the positively stained chromatin exhibited a tangled globular-like structure. Bar, 5 μm. (C) Chromatin fibers fold into hierarchically different structures. After mounting the chromatin fiber on the continuous carbon coated EM girds and further using the buffer to align chromatin fibers along a specific direction by placing a filter paper at the edge of the grid to absorb the buffer, the weak force provided by the buffer flow extends the chromatin. The extended chromatin fibers with length as long as 100 μm hierarchically folds into different structures. (D) The beads-on-a-string structure of 10 nm chromatin fibers. Nucleosome-like particles were connected by linker DNA on a replication fork-like structure. The image contrast was reversed in order to present the “nucleosome-like” particles. White dots are gold nanoparticles used as fiducial marker for electron tomography. Bar, 50 nm.

Author Manuscript Author Manuscript Author Manuscript Author Manuscript

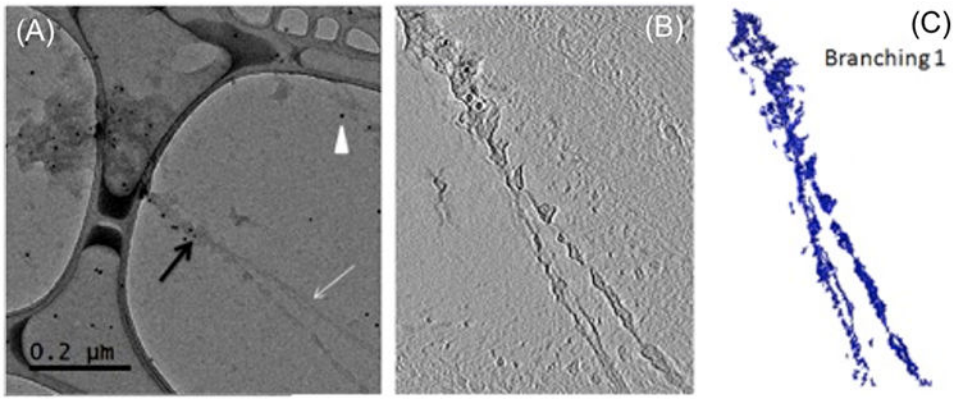

Figure 2.

CryoET of transition structure from the 30 nm to the 10 nm chromatin fiber. (A) Cryo-ET image of MCF7 Interphase chromatin with EM stage tilted at 0 degree. Black arrow indicates the root of branching structure while the white arrow indicates one of the branches of the branching structure. The white arrowhead indicates 10 nm gold nanoparticle used as fiducial marker in Cryo-ET. (B) Tomographic slice of the chromatin transition structure. The CryoET data from −56 to +56 degree was reconstructed by IMOD. (C) Image segmentation of the chromatin transition structure using Chimera.

Author Manuscript Author Manuscript Author Manuscript Author Manuscript

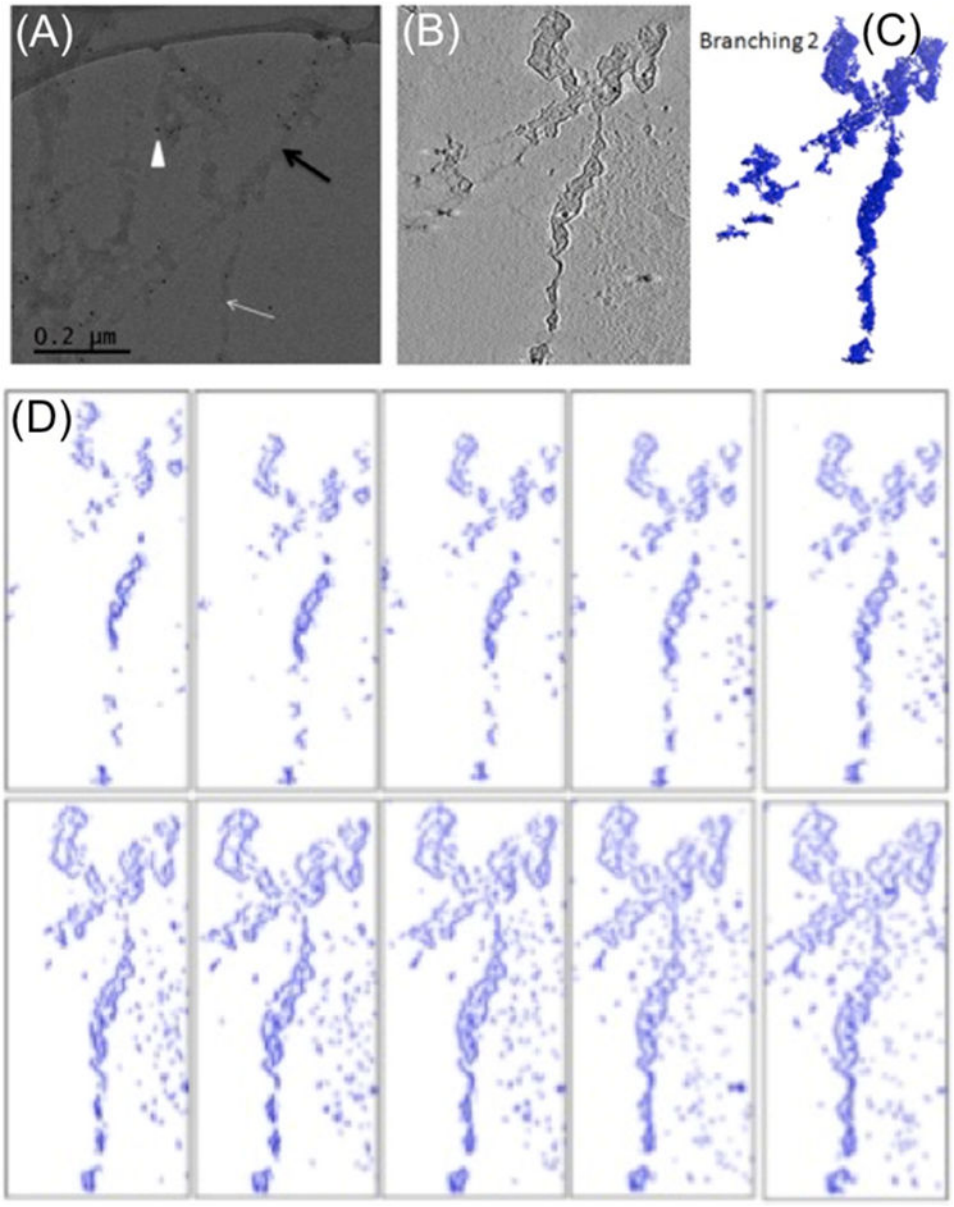

Figure 3.

CryoET of transition structure from the 30 nm to 10 nm chromatin fiber and chromatin helix structure. (A) Cryo-ET image of MCF7 Interphase chromatin, tilted at 0 degree. Black arrow indicates the root of the branching structure, and the white arrow indicates one of the branches of the branching structure. The white arrowhead indicates 10 nm gold nanoparticle used as fiducial marker in Cryo-ET. (B) Tomographic slice of the chromatin transition structure. (C) Image segmentation of the chromatin transition structure using Chimera. (D) Observed chromatin helical ribbon structures. Continuous image segmentation of tomography slices using Chimera.

Author Manuscript

Author Manuscript

Author Manuscript

Author Manuscript

Table 1

Comparison of observed helical structures with Li-Zhu 30 nm chromatin model

	Root (nm)	Branch (nm)	Helix thickness (nm)	Helix Length (nm)
Branching 1	38.5	18.7	18.7	59.3
Branching 2	31.2	15.6	11.4	56.2
Li-Zhu style	NA	NA	27.2	55.8